

Interface-plane parameterization for macroscopic grain boundary identification

A. Morawiec

Institute of Metallurgy and Materials Science, Polish Academy of Sciences,
Kraków, Poland.

E-mail: nmmorawi@cyf-kr.edu.pl

Tel.: ++48-122952854, Fax: ++48-122952804

Abstract

The geometric state of a flat boundary is frequently described using the so-called macroscopic parameters. They are a principal tool for dealing with interfaces at the continuous scale. The paper describes a new method for macroscopic identification of boundaries. The proposed approach is based on Euler angles representing orientations of the crystals. Two pairs of the angles are directly related to two vectors normal to the boundary plane in the crystal reference frames, and the new boundary representation can be viewed as a triplet composed of these vectors and the angle of rotation about the axis perpendicular to the plane. The representation resembles the ‘interface-plane scheme’, but unlike the latter, it is a proper parameterization. Basic practical aspects of the parameterization (such as equivalences due to symmetries, fundamental regions, uniform distribution of boundaries) are considered. The parameterization is applied to examination of Bulatov-Reed-Kumar model of grain boundary energy and reveals its previously unknown features. The proposed boundary identification method, apart from its use in numerical calculations, appeals to physical intuition.

Keywords: Misorientation; Grain boundary plane; Anisotropy; Modeling; Grain boundary energy;

March 28, 2025

1 Introduction

Quantities that identify boundary types and enable them to be distinguished are essential for the study of grain boundaries. The basic method of describing a planar boundary is to give the misorientation between the crystals and the orientation of the boundary plane [1–4]. From the atomistic viewpoint, the purely geometric macroscopic concept of a flat zero-thickness boundary is meaningless, but in practice, details of boundary structures and atomic-scale translations are often inaccessible. In particular, only the macroscopic description is possible when experimental data on boundaries are limited to approximate boundary locations and grain orientations. The macroscopic approximation, while avoiding the complexity that would arise if atomic positions or microscopic data were considered, takes into account crystal anisotropy, which is important for explaining boundary properties.

The five real variables specifying grain misorientation and boundary plane are referred to as macroscopic boundary parameters. A parameterization must be an onto mapping, i.e., first, each set of parameters is assigned to exactly one boundary type, and second, for every boundary configuration there exists a set of parameters assigned to it. The macroscopic boundary parameters work behind the scenes in software dealing with boundary data sets. They are used to characterize experimental results (e.g., [5–7]), in boundary simulations (e.g., [8, 9]), in modeling of microstructures (e.g., [10, 11]), and in many other studies on properties of boundary networks (e.g., [12, 13]).

Numerous papers on grain boundaries emphasize the importance of crystal planes on both sides of the boundary. Some approaches – from Pumphray’s ‘plane matching theory’ [14], through the idea of ‘special boundary planes’ [15, 16], to the recently promoted ‘grain boundary inter-connection’ [17–19] – are focused on the crystal planes. In such cases, the most appropriate boundary parameterization would be one that is based directly on parameters of the boundary planes. Boundaries in bicrystals are often characterized by Miller indices of abutting crystal planes. This description is incomplete, but it brings to mind an attractive boundary parameterization. The idea is to use parameters of the boundary plane with respect to reference frames of the two crystals and a fifth parameter – the angle, say χ , of a rotation about axis perpendicular to the plane. The concept is intuitively simple, clear and compelling, but the practical problem of precisely defining such parameters has eluded researchers. Wolf and Lutsko introduced the ‘interface-plane scheme’ based on a triplet consisting of two vectors representing the boundary plane in reference frames of the crystals on both sides of the boundary and a ‘twist’ angle [20].¹ However, the interface-plane scheme

¹See also [21] where relationships defining the interface-plane scheme were completed and [22] for a more general approach to the boundary decomposition into ‘twist’ and ‘tilt’.

is not a proper parameterization because some physically distinct boundaries correspond to the same triplets [23].

This paper describes five quantities, two pairs characterizing the boundary plane with respect to the crystal reference frames and an additional angle, which together constitute a proper parameterization. The parameters can be interpreted as Euler angles related to orientations of the crystals or, more conveniently, they can be viewed as a triplet composed of two vectors identifying the orientation of the boundary plane in the crystals and the angle of rotation about an axis perpendicular to the plane. This new boundary representation will be called the ‘interface-plane parameterization’.

The remainder of this paper is organized as follows. After recalling some basics and establishing the notation, the five parameters are defined, and they are linked to unit vectors normal to the boundary plane in the reference frames of the crystals. Next, aspects important for practical applications of the interface-plane parameterization are presented: sets of parameters equivalent due to symmetries and fundamental regions with representatives of the equivalence classes are considered, forms of interface-plane parameters of characteristic boundaries are described, and a model of uniform boundary distribution is briefly discussed. Before concluding, the new parameterization is applied to examination of a model of grain boundary energy. For simplicity, the considerations below are limited to the case of homophase interfaces between centrosymmetric crystals.

2 Preliminaries

2.1 Ways to represent grain boundaries

Practical methods of representing boundaries by the misorientation/plane pair take various specific forms because there are many ways to describe misorientations and plane orientations. When the boundary plane is given in the reference frame of one of the crystals, the description based on the misorientation and plane is ‘asymmetric’. To make the representation more complete and symmetric, it is necessary to somehow incorporate information about orientation of the plane with respect to the other crystal.

Such information is contained in a 4×4 interface matrix built of a 3×3 matrix representing the misorientation and boundary plane normals in reference frames of both crystals [24–26]. When generating input for atomistic simulations, the natural specification of boundaries relies on pairs of crystal orientations in a configuration in which the boundary plane has a fixed orientation in the simulation box. In this context, Olmsted proposed to use pairs of orientation matrices [27]. Olmsted’s pairs of matrices were replaced by pairs

of unit quaternions in [28]. These extensive boundary representations are convenient in computations, but they are practically useless in interpersonal communication because of abundance of numbers involved or intricate interpretation. Sutton and Balluffi [29] proposed representing boundaries by misorientation and the linear combination $(\mathbf{n} + \mathbf{n}')/2$, where \mathbf{n} and \mathbf{n}' contain components of the unit vector normal to the boundary plane in the reference frames of the two crystals, but the combination is not directly interpretable; one needs to refer to misorientation to get Miller indices of the boundary plane.

2.2 Rotation matrices

When dealing with crystal orientations, it is convenient to follow the Bunge's convention [30] used in texture analysis and EBSD orientation mapping systems. Orientations are identified with rotations relating Cartesian reference frames ascribed to the crystals and to the sample. The rotation about axis along the unit vector $\mathbf{k} = [k^1 \ k^2 \ k^3]^T$ by the angle ω is represented by a 3×3 special orthogonal matrix $R(\mathbf{k}, \omega) = I \cos \omega + \mathbf{k} \otimes \mathbf{k} (1 - \cos \omega) + \mathbf{rot}(\mathbf{k}) \sin \omega$, where the entries ij of the identity matrix I , $\mathbf{k} \otimes \mathbf{k}$ and $\mathbf{rot}(\mathbf{k})$ are δ_{ij} , $k^i k^j$ and $\sum_l \varepsilon_{ijl} k^l$, respectively.

In Bunge's convention, if the crystal orientation is represented by the matrix g and the column array \mathbf{n}_s contains vector coordinates in the sample reference frame, the coordinates in the crystal reference frame are $g\mathbf{n}_s$. The orientation matrix g is usually parameterized using Euler angles φ_1 , ϕ and φ_2

$$g = R(\varphi_1, \phi, \varphi_2) = R(\mathbf{e}_z, \varphi_2)R(\mathbf{e}_x, \phi)R(\mathbf{e}_z, \varphi_1) ,$$

where $\mathbf{e}_x = [1 \ 0 \ 0]^T$ and $\mathbf{e}_z = [0 \ 0 \ 1]^T$. Here, the notation is abused by using the same symbol R for $R(\mathbf{k}, \omega)$ and $R(\varphi_1, \phi, \varphi_2)$, but the meaning of the symbol can be easily inferred from the number and type of arguments. Using $Q(\phi, \varphi_2) = R(0, \phi, \varphi_2)$, one also has $R(\varphi_1, \phi, \varphi_2) = Q(\phi, \varphi_2)R(\mathbf{e}_z, \varphi_1)$.

In calculations involving the interface matrices, it is convenient to use a 4×4 representation of rotations [24–26]. The matrix corresponding to (\mathbf{k}, ω) is given by

$$\mathbf{R}(\mathbf{k}, \omega) = \left[\begin{array}{c|c} 1 & \mathbf{0}^T \\ \hline \mathbf{0} & R(\mathbf{k}, \omega) \end{array} \right] , \quad (1)$$

where $\mathbf{0} = [0 \ 0 \ 0]^T$. If the arguments of \mathbf{R} are three angles, the symbol denotes $\mathbf{R}(\varphi_1, \phi, \varphi_2) = \mathbf{R}(\mathbf{e}_z, \varphi_2)\mathbf{R}(\mathbf{e}_x, \phi)\mathbf{R}(\mathbf{e}_z, \varphi_1) = \mathbf{Q}(\phi, \varphi_2)\mathbf{R}(\mathbf{e}_z, \varphi_1)$, where $\mathbf{Q}(\phi, \varphi_2) = \mathbf{R}(0, \phi, \varphi_2)$.

2.3 Interface matrix

The misorientation between crystals 1 and 2, understood as a rotation relating the orientation g_2 of crystal 2 to the orientation g_1 of crystal 1, is represented by the matrix $M = g_1 g_2^T$. The boundary plane can be specified by the unit vector \mathbf{n}_1 normal to the plane and directed (by convention) towards the crystal 2, with coordinates given in the Cartesian reference frame of crystal 1. The pair (M, \mathbf{n}_1) unambiguously determines the macroscopic boundary geometry. The same boundary seen from the viewpoint of the other crystal is determined by (M^T, \mathbf{n}_2) , where the vector $\mathbf{n}_2 = -M^T \mathbf{n}_1$ is directed towards the crystal 1 and has coordinates given in the reference frame of crystal 2. The interface matrix [24–26] encompasses all M , \mathbf{n}_1 and \mathbf{n}_2 : the matrix $\tilde{\mathbf{B}}$ representing the boundary between crystals 1 and 2 is defined as

$$\tilde{\mathbf{B}} = \mathbf{B}(M, \mathbf{n}_1) = \left[\begin{array}{c|c} 1 & \mathbf{n}_2^T \\ \hline \mathbf{n}_1 & M \end{array} \right]. \quad (2)$$

The boundary between crystals 2 and 1 is represented by $\tilde{\mathbf{B}}^T$.

Let the 4×4 matrices \mathbf{R}_i ($i = 1, 2$) be related to 3×3 matrices R_i via (1). If crystal 1 is rotated by R_1 , then g_1 and \mathbf{n}_1 become $R_1 g_1$ and $R_1 \mathbf{n}_1$, respectively. An analogous remark applies to crystal 2. Thus, rotations of crystal 1 by \mathbf{R}_1 and crystal 2 by \mathbf{R}_2 change the boundary represented by $\mathbf{B}(M, \mathbf{n}_1)$ to the boundary represented by $\mathbf{B}(R_1 M R_2^T, R_1 \mathbf{n}_1) = \mathbf{R}_1 \mathbf{B}(M, \mathbf{n}_1) \mathbf{R}_2^T$. This observation is convenient for taking into account crystal symmetries [24, 25]. Below, it is used for defining the new parameterization.

3 The interface-plane parameterization

3.1 Relationships defining the parameterization

Let \mathbf{B}_0 denote the interface matrix $\mathbf{B}(I, \mathbf{e}_z)$. Physically, \mathbf{B}_0 represents a configuration in which the first crystal occupies the region with $z < 0$ and the second crystal with the same orientation occupies the region with $z > 0$. An arbitrary interface matrix $\tilde{\mathbf{B}}$ can be expressed as

$$\tilde{\mathbf{B}} = \mathbf{R}_1 \mathbf{B}_0 \mathbf{R}_2^T. \quad (3)$$

This relationship reflects the fact that an arbitrary boundary can be obtained by rotating the crystals forming the configuration represented by \mathbf{B}_0 .

The matrices \mathbf{R}_i ($i = 1, 2$) are directly related to Olmsted’s rotation matrices defined in [27]. It must be emphasized that these are not orientation matrices obtained from an experiment. The experimental data must be rotated to the configuration with the boundary plane normal to the sample’s z -direction. (The unit vector \mathbf{n}_s normal to the boundary plane

and directed outward from crystal 1, with components in the sample reference frame, is transformed to \mathbf{e}_z by $R_0 = R(\widehat{\mathbf{k}}_0, \omega_0)$ such that $\widehat{\mathbf{k}}_0$ is the normalized $\mathbf{k}_0 = \mathbf{e}_z \times \mathbf{n}_s$ and $\omega_0 = \arccos(\mathbf{e}_z \cdot \mathbf{n}_s)$ if $\mathbf{n}_s \neq \pm \mathbf{e}_z$, $\widehat{\mathbf{k}}_0$ is an arbitrary unit vector perpendicular to \mathbf{e}_z and $\omega_0 = \pi$ if $\mathbf{n}_s = -\mathbf{e}_z$, and $R_0 = I$ if $\mathbf{n}_s = +\mathbf{e}_z$. One has $R_0 \mathbf{n}_s = \mathbf{e}_z$. If experimentally obtained orientation of crystal i is g_i ($i = 1, 2$), then the matrices \mathbf{R}_i used in (3) correspond to $R_i = g_i R_0^T$.)

In the following, Euler angles parameterizing the rotations \mathbf{R}_i will be needed. The symbols φ_1 , ϕ and φ_2 are conventionally used for Euler angles of crystal orientations in the sample (i.e. for g_i). To avoid confusion, the Euler angles of \mathbf{R}_i will be denoted by χ_i , θ_i and ψ_i , i.e., $\mathbf{R}_i = \mathbf{R}(\chi_i, \theta_i, \psi_i)$. In this notation, (3) has the form

$$\begin{aligned} \tilde{\mathbf{B}} &= \mathbf{R}(\chi_1, \theta_1, \psi_1) \mathbf{B}_0 \mathbf{R}(\chi_2, \theta_2, \psi_2)^T \\ &= \mathbf{Q}(\theta_1, \psi_1) \mathbf{R}(\mathbf{e}_z, \chi_1) \mathbf{B}(I, \mathbf{e}_z) \mathbf{R}(\mathbf{e}_z, \chi_2)^T \mathbf{Q}(\theta_2, \psi_2)^T, \end{aligned}$$

and since $\mathbf{R}(\mathbf{e}_z, \chi_1) \mathbf{B}(I, \mathbf{e}_z) \mathbf{R}(\mathbf{e}_z, \chi_2)^T = \mathbf{B}(R(\mathbf{e}_z, \chi_1 - \chi_2), \mathbf{e}_z)$, one obtains

$$\tilde{\mathbf{B}} = \mathbf{Q}(\theta_1, \psi_1) \mathbf{B}(R(\mathbf{e}_z, \chi), \mathbf{e}_z) \mathbf{Q}(\theta_2, \psi_2)^T, \quad (4)$$

where $\chi = \chi_1 - \chi_2$. Thus, the interface matrix $\tilde{\mathbf{B}}$ is expressed via five independent quantities: $\theta_1, \psi_1, \chi, \theta_2, \psi_2$. As (4) can also be written in the form $\tilde{\mathbf{B}} = \mathbf{R}(\chi, \theta_1, \psi_1) \mathbf{B}_0 \mathbf{R}(0, \theta_2, \psi_2)^T$, χ can be interpreted as an Euler angle. (See Fig. 1.) Formulae for inverting eq.(4), i.e. for getting $\theta_1, \psi_1, \chi, \theta_2, \psi_2$ from $\tilde{\mathbf{B}}$, are listed in Appendix A.

From eq.(4) it follows that the first column of $\tilde{\mathbf{B}}$ is determined by $\mathbf{Q}(\theta_1, \psi_1)$ and the first row is determined by $\mathbf{Q}(\theta_2, \psi_2)$. Hence, based on (2), the vectors \mathbf{n}_1 and \mathbf{n}_2 are expressible through θ_1, ψ_1 and θ_2, ψ_2 , respectively. They are given by $\mathbf{n}_1 = +Q(\theta_1, \psi_1)\mathbf{e}_z$ and $\mathbf{n}_2 = -Q(\theta_2, \psi_2)\mathbf{e}_z$, or by

$$\mathbf{n}_1 = +\Theta(\theta_1, \pi/2 - \psi_1) \quad \text{and} \quad \mathbf{n}_2 = -\Theta(\theta_2, \pi/2 - \psi_2), \quad (5)$$

where the function Θ relates the unit vector \mathbf{n} to its spherical coordinates (θ, φ) in the conventional way

$$\mathbf{n} = \Theta(\theta, \varphi) = [\cos \varphi \sin \theta \quad \sin \varphi \sin \theta \quad \cos \theta]^T. \quad (6)$$

Instead of dealing with the quintuple $(\theta_1, \psi_1, \chi, \theta_2, \psi_2)$, it is more convenient to use the triplet $(\mathbf{n}_1, \chi, \mathbf{n}_2)$. This representation resembles the interface-plane scheme [20]. However, unlike the interface-plane scheme, it is a proper parameterization: every macroscopic boundary configuration is represented by a triplet, and no two macroscopically distinct boundaries correspond to the same triplet. In the case of zero misorientation angle, i.e., when $M = I$, one has $\mathbf{n}_1 = -\mathbf{n}_2$ and $\chi = 0$ or the triplet $(\mathbf{n}, 0, -\mathbf{n})$, where \mathbf{n} is an arbitrary unit vector.

Such parameters do not represent true boundaries, but the considerations below are simpler if they are not excluded.

Although the parameter χ can be changed without affecting the crystal planes forming the boundary, it is not determined solely by the misorientation. In other words, boundaries with the same misorientation and different plane inclinations generally have different values of χ . The configuration with $\chi = 0$ corresponds to the misorientation represented by $R(-\psi_2, \theta_1 - \theta_2, \psi_1)$.

Planes spanned by vectors of the direct crystal lattice can be represented by Miller indices. Let \mathbf{n} be perpendicular to such a plane. To describe interfaces, Miller indices can be defined as integers $(hkl) = (h_1 h_2 h_3)$ such that $h_j = \lambda \mathbf{n} \cdot \mathbf{a}_j$ or $\mathbf{n} = \sum_j h_j \mathbf{a}^j / \lambda$, where \mathbf{a}_j (\mathbf{a}^j) denotes the j -th basis vector of the direct (reciprocal) crystal lattice, and the real coefficient λ is positive. If the plane of the boundary $(\mathbf{n}_1, \chi, \mathbf{n}_2)$ is expressible through Miller indices in each of the neighboring crystals, the boundary can be represented by

$$((hkl)_1, \chi, (hkl)_2) ,$$

where the Miller indices $(hkl)_i$ replaced the corresponding vector \mathbf{n}_i .

3.2 Example

It is worth illustrating the above considerations with an example. Let the crystals have cubic $m\bar{3}m$ symmetry, and let axes of the crystal Cartesian coordinates systems be along four-fold symmetry axes. The twin boundary common in fcc metals separates crystals misoriented by the half-turn about $\mathbf{k} = [111]^T / \sqrt{3}$, and the boundary plane is perpendicular to $\mathbf{n}_1 = [111]^T / \sqrt{3}$. The corresponding interface matrix has the form

$$\mathbf{B}(R(\mathbf{k}, \pi), \mathbf{n}_1) = \frac{1}{3} \left[\begin{array}{c|ccc} 1 & -\sqrt{3} & -\sqrt{3} & -\sqrt{3} \\ \hline \sqrt{3} & -1 & 2 & 2 \\ \sqrt{3} & 2 & -1 & 2 \\ \sqrt{3} & 2 & 2 & -1 \end{array} \right] .$$

Hence, one has

$$(\theta_1, \psi_1, \chi, \theta_2, \psi_2) = \left(\arctan \sqrt{2}, \pi/4, \pi, \arctan \sqrt{2}, \pi/4 \right) ,$$

or easier to interpret $(\mathbf{n}_1, \chi, \mathbf{n}_2) = ([111]^T / \sqrt{3}, \pi, -[111]^T / \sqrt{3})$. Replacing the normalized vectors \mathbf{n}_i with Miller indices gives

$$(\mathbf{n}_1, \chi, \mathbf{n}_2) \sim ((111), \pi, (\bar{1}\bar{1}\bar{1})) .$$

Due to crystal symmetry, this is one of several equivalent representations of the twin boundary.

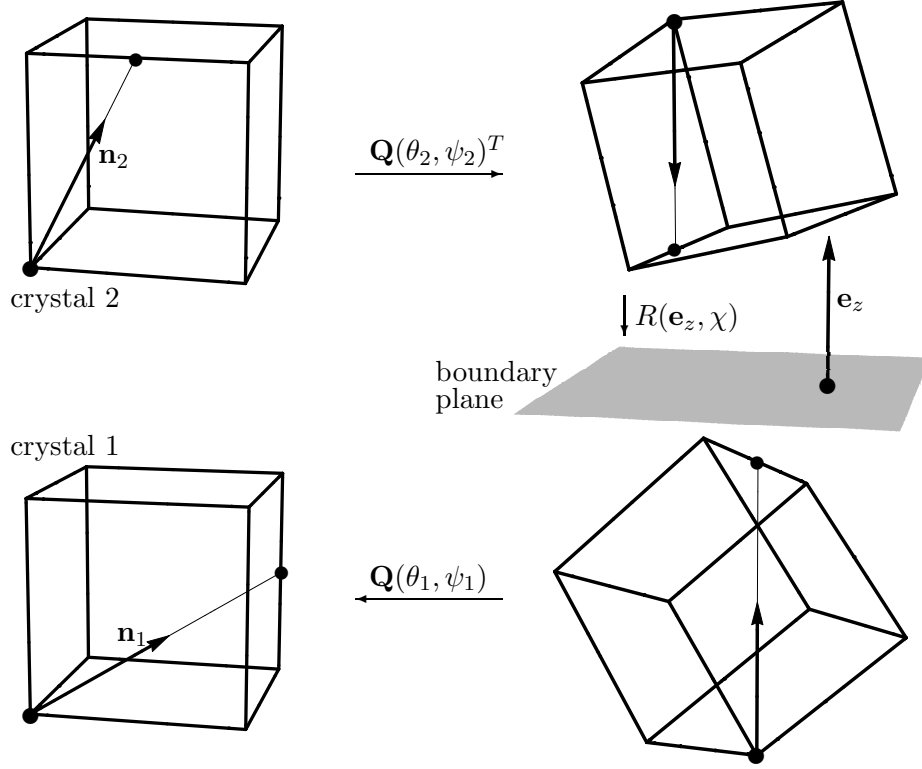


Figure 1: Schematic illustration of the configuration used for defining the interface-plane parameters (in the case of cubic crystals). Coordinates of the vectors \mathbf{n}_i in the Cartesian reference frames linked to the crystals are related to (θ_i, ψ_i) via eq.(5) and χ is the angle of rotation about normal to the boundary plane \mathbf{e}_z .

3.3 Equivalences due to symmetries

Because of symmetries, different sets of parameters stand for the same macroscopic boundary configuration. The solution to the problem of equivalent descriptions of boundaries between centrosymmetric crystals is given in [24]; see also [25]. The equivalences listed there can be easily rewritten in the new formalism. The assumption that the crystal point group contains inversion means that

$$(\mathbf{n}_1, \chi, \mathbf{n}_2) \simeq (-\mathbf{n}_1, -\chi, -\mathbf{n}_2) , \quad (7)$$

where \simeq stands for equivalence. With C_1 and C_2 denoting matrices representing proper rotations in the point group of the crystal, one has

$$(\mathbf{n}_1, \chi, \mathbf{n}_2) \simeq (C_1 \mathbf{n}_1, \chi', C_2 \mathbf{n}_2) , \quad (8)$$

where χ' , in general, differs from χ . The most convenient way to determine χ' is to transform $(\mathbf{n}_1, \chi, \mathbf{n}_2)$ to $\tilde{\mathbf{B}}$, get $\tilde{\mathbf{B}}' = C_1 \tilde{\mathbf{B}} C_2^T \simeq \tilde{\mathbf{B}}$, and transform $\tilde{\mathbf{B}}'$ back to $(C_1 \mathbf{n}_1, \chi', C_2 \mathbf{n}_2)$; C_i is the 4×4 matrix related to C_i via eq.(1).

The equivalences (7) and (8) arise from the symmetry of the crystal and are therefore inevitable. Depending on circumstances, one may or may not allow for grain exchange symmetry. Allowing this symmetry means that the boundary between grains 1 and 2 is identified with the boundary between grains 2 and 1. In terms of the interface-plane parameters, the grain exchange symmetry has the form

$$(\mathbf{n}_1, \chi, \mathbf{n}_2) \simeq (\mathbf{n}_2, \chi, \mathbf{n}_1) . \quad (9)$$

Like (7) and (8), also this relationship follows directly from the corresponding equivalence expressed via interface matrices in [24].

It is worth stating explicitly that, in general, the triplet $(\mathbf{n}_1, \chi, \mathbf{n}_2)$ is not equivalent to $(\mathbf{n}_1, \chi', -\mathbf{n}_2)$. More precisely, if none of the vectors \mathbf{n}_i is transformed to $-\mathbf{n}_i$ by a symmetry operation being a proper rotation, then there are no such χ and χ' that $(\mathbf{n}_1, \chi, \mathbf{n}_2) \simeq (\mathbf{n}_1, \chi', -\mathbf{n}_2)$. For example, if crystals have $m\bar{3}m$ symmetry, the representation $((1\ 2\ 3), \chi, (3\ 5\ 7))$ is never equivalent to $((1\ 2\ 3), \chi', (\bar{3}\ \bar{5}\ \bar{7}))$. Similarly, $((1\ 2\ 3), \chi, (3\ 5\ 7))$ is never equivalent to $((1\ 2\ 3), \chi', (7\ 5\ 3))$. In view of the above, it is clear that if boundary planes are represented by Miller indices, a distinction must be made between $(h\ k\ l)$ and $(\bar{h}\ \bar{k}\ \bar{l})$, and between different sequences of indices. Awareness of this fact is not widespread among those working on cubic materials. It is symptomatic that the works focused on pairs of crystal planes forming a boundary (e.g., [15–19]) ignore the necessity of making such distinctions. This necessity is somewhat hidden when boundaries are represented by misorientation/plane pairs, but is evident when the interface-plane parameterization is used.

Based on (7) and (8), it can be verified that the representations equivalent to the example twin boundary $(\mathbf{n}_1, \chi, \mathbf{n}_2) \sim ((1\ 1\ 1), \pi, (\bar{1}\ \bar{1}\ \bar{1}))$ described in section 3.2 have the forms

$$((h\ k\ l), j\pi/3, (h'\ k'\ l')) , \quad (10)$$

where the indices h, k, l, h', k', l' take the values of ± 1 , $j = 0, 1, \dots, 5$, and the condition $ll' = 1 - 2 \bmod(j, 2)$ is satisfied, i.e., $ll' = +1$ when j is even, and $ll' = -1$ when j is odd. For instance, with all Miller indices equal to $+1$ and $j = 0$, one has

$$((1\ 1\ 1), \pi, (\bar{1}\ \bar{1}\ \bar{1})) \simeq ((1\ 1\ 1), 0, (1\ 1\ 1)) . \quad (11)$$

The number of distinct representations (10) is $2^6 \times 3 = 192$. The number of proper rotations in the point group $m\bar{3}m$ is $N_p = 24$, and the number of equivalent representations of a general boundary is $2 \times N_p^2 = 1152$. Thus, the case of twin boundary is degenerate, and the degree of degeneracy is 6.

3.4 Fundamental region

Since each of the vectors \mathbf{n}_1 and \mathbf{n}_2 covers the unit sphere S^2 and χ covers the circle S^1 , the domain D of the triplets $(\mathbf{n}_1, \chi, \mathbf{n}_2)$ is the Cartesian product $S^2 \times S^1 \times S^2$. Due to symmetries, physical boundaries correspond to classes of equivalent parameters. These classes are analogous to classes of equivalent crystallographic directions or equivalent orientations typically dealt with in texture analysis. In such cases, computations rely on representatives of equivalence classes. It is convenient to specify the part of the domain D in which these representatives are gathered [25]. Such part is known as the fundamental region. It is a closed subset of D such that the images of the subset due to the symmetries cover D , and the interiors of the images have no common points. Determination of fundamental regions for $(\mathbf{n}_1, \chi, \mathbf{n}_2)$ -parameterized boundaries relies on fundamental regions for crystallographic directions.

For illustration, inequalities determining a fundamental region for $m\bar{3}m$ crystal symmetry will be described. In this case, the fundamental region for crystallographic directions is known as the standard stereographic triangle (SST). It can be defined as a set of directions $\mathbf{n}_i = [n_i^1 \ n_i^2 \ n_i^3]^T$ ($i = 1, 2$) satisfying the conditions $n_i^3 \geq n_i^2 \geq n_i^1 \geq 0$. Proper rotations of $m\bar{3}m$ constitute the point group 432, for which the fundamental region of directions consists of the double standard stereographic triangle (DSST); the latter can be defined by the inequalities $n_i^3 \geq n_i^k \geq 0$, where $k = 1, 2$.

If only the equivalences (8) are used, the fundamental region for $(\mathbf{n}_1, \chi, \mathbf{n}_2)$ is $\text{DSST} \times S^1 \times \text{DSST}$, and eq.(7) reduces it further to

$$\text{DSST} \times S^1_{\perp} \times \text{DSST} , \quad (12)$$

where S^1_{\perp} denotes the semicircle defined by χ ranging from 0 to π ; see Fig. 2.

The choice of the fundamental region is not unique. The region (12) can be replaced by $\text{SST} \times S^1 \times \text{DSST}$ or $\text{DSST} \times S^1 \times \text{SST}$. Yet another option is to use $\text{DSST} \times S^1 \times \text{DSST}$ with the condition $n_1^1 - n_1^2 \geq n_2^1 - n_2^2$, but it must be noted that the form of this condition depends on the inequalities defining DSST.² The latter option is mentioned because a similar scheme is necessary to account for grain exchange symmetry.

If besides (7) and (8) also the grain exchange symmetry (9) holds, the fundamental region for interface-plane parameters is $\text{DSST} \times S^1 \times \text{DSST}$ with the conditions $n_1^1 - n_1^2 \geq n_2^1 - n_2^2$ and $n_1^1 + n_1^2 \geq n_2^1 + n_2^2$.³

These expressions for the fundamental regions were confirmed by numerical tests.

²For instance, if DSST is defined by $n_i^3 \geq n_i^2 \geq |n_i^1|$, one can use the condition $n_1^1 \geq n_2^1$.

³If DSST is defined by $n_i^3 \geq n_i^2 \geq |n_i^1|$, one can use the conditions $n_1^1 \geq n_2^1$ and $n_1^2 \geq n_2^2$.

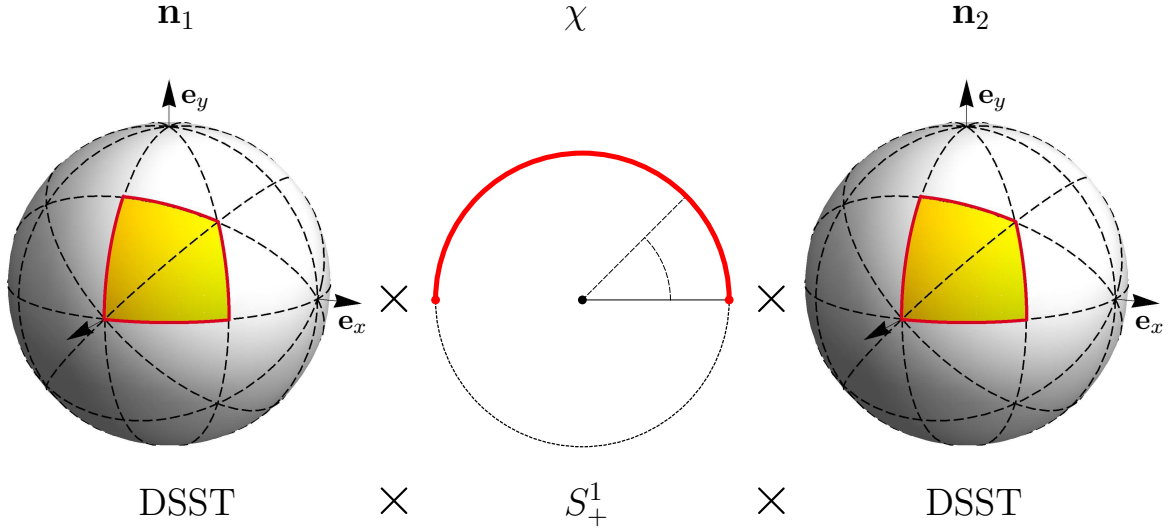


Figure 2: Schematic illustration of the fundamental region (12) for $(\mathbf{n}_1, \chi, \mathbf{n}_2)$ -parameterized boundaries between crystals with $m\bar{3}m$ symmetry. This region concerns the mandatory equivalences (7) and (8). The areas marked on the spheres are double standard stereographic triangles defined by $n_i^3 \geq n_i^k \geq 0$, where $i = 1, 2$ and $k = 1, 2$.

3.5 Characteristic boundaries

Characteristic boundaries have special arrangements of boundary planes and misorientation axes. Usually, specifications of such boundaries concern low-index cases, but formal definitions ignore magnitudes of the indices. In particular, a boundary having a representation with the misorientation axis perpendicular (parallel) to the boundary plane is a twist (tilt) boundary. A boundary is symmetric when the boundary plane is a mirror plane between crystal structures.

The interface-plane parameters of twist and symmetric boundaries are simple. A symmetric boundary is represented by

$$(\mathbf{n}, \pi, -\mathbf{n}),$$

and every triplet having this form represents a symmetric boundary. Such a boundary is determined by \mathbf{n} , i.e., by two independent quantities [23]. The triplet

$$(\mathbf{n}, \chi, -\mathbf{n}) \tag{13}$$

represents a twist boundary. The misorientation angle of a boundary represented by $(\mathbf{n}, \chi, -\mathbf{n})$ is $\arccos(\cos \chi)$, and its misorientation axis is $\text{sign}(\sin \chi) \mathbf{n}$ if χ differs from 0 and π ; the axis is $\pm \mathbf{n}$ if $\chi = \pi$, and is arbitrary if $\chi = 0$. The misorientation angle of a boundary represented by

$$(\mathbf{n}, \chi, +\mathbf{n}) \tag{14}$$

is π , and its misorientation axis is perpendicular to \mathbf{n} , i.e., (14) represents a 180° -tilt boundary. Every 180° -tilt boundary has a representation of this form. Boundaries represented by triplets of types (13) and (14) are determined by three independent quantities [23].

Representations of general tilt boundaries are more complex; see, Appendix B. For a boundary to be called a tilt boundary, it must satisfy one scalar condition, therefore tilt boundaries form a four-dimensional subspace of all boundaries.

Clearly, when characterizing experimental boundary data, it is not enough to look at a single set of parameters, but one also needs to consider symmetrically equivalent configurations. E.g., in order to test whether the boundary with parameters $(\mathbf{n}_1, \chi, \mathbf{n}_2)$ is a twist boundary, one needs to check not only if $\mathbf{n}_1 \approx -\mathbf{n}_2$, but also whether there are C_1 and C_2 such that $C_1 \mathbf{n}_1 \approx -C_2 \mathbf{n}_2$. Taking this into account, it is easy to see that a given boundary can have several attributes, e.g., it can be a twist as well as a tilt boundary [31]. A prime example of this case is the twin boundary described in section 3.2; its equivalent representations (11) have the forms (13) and (14).

3.6 Uniform boundary distribution

One of the basic characteristics of boundary networks in polycrystalline materials is the frequency of occurrence of particular boundary types [32]. For gauging the frequencies, a model representing the uniform distribution of boundaries is needed. The model is directly linked to the method of generating uniformly distributed ('random') boundaries.

The simplest and convenient model assumes that a random boundary is obtained by using a random misorientation and a random boundary plane [25]. The question is how this model translates to the parameterization by $(\mathbf{n}_1, \chi, \mathbf{n}_2)$? Based on properties of proper rotations (representing misorientations), the model corresponds to uniform distributions of \mathbf{n}_1 and \mathbf{n}_2 on the sphere S^2 and uniform distribution of χ on the circle S^1 . In other words, if the triplet $(\mathbf{n}_1, \chi, \mathbf{n}_2)$ representing a random boundary is needed, it is enough to generate random directions \mathbf{n}_1 and \mathbf{n}_2 , and a random angle χ . Technically, with $\text{rnd}(a, b)$ denoting a random real number between a and b , the random directions are $\mathbf{n}_i = \Theta(\theta_i, \psi_i)$, where $\theta_i = \arccos \text{rnd}(-1, 1)$ and $\psi_i = \text{rnd}(0, 2\pi)$, and $\chi = \text{rnd}(0, 2\pi)$.

The above model of uniformity is related to the differential volume element dV , which is a tool for integrating functions over macroscopic boundary parameters. It is given by

$$dV = d\mathbf{n}_1 d\mathbf{n}_2 d\chi / (2\pi) = \sin \theta_1 \sin \theta_2 d\theta_1 d\psi_1 d\chi d\theta_2 d\psi_2 / (32\pi^3) .$$

This expression follows directly from the formula for area element on unit sphere in spherical coordinates.

4 Grain boundary energy versus interface-plane parameters

Parameterizations of grain boundaries allow for estimating the dependence of boundary properties on boundary types. In this way, grain boundary populations, energies and curvatures as functions of grain misorientation and boundary plane have been evaluated; see, e.g., [32–34]. Using different parameterizations allows for looking at these functions from different perspectives.

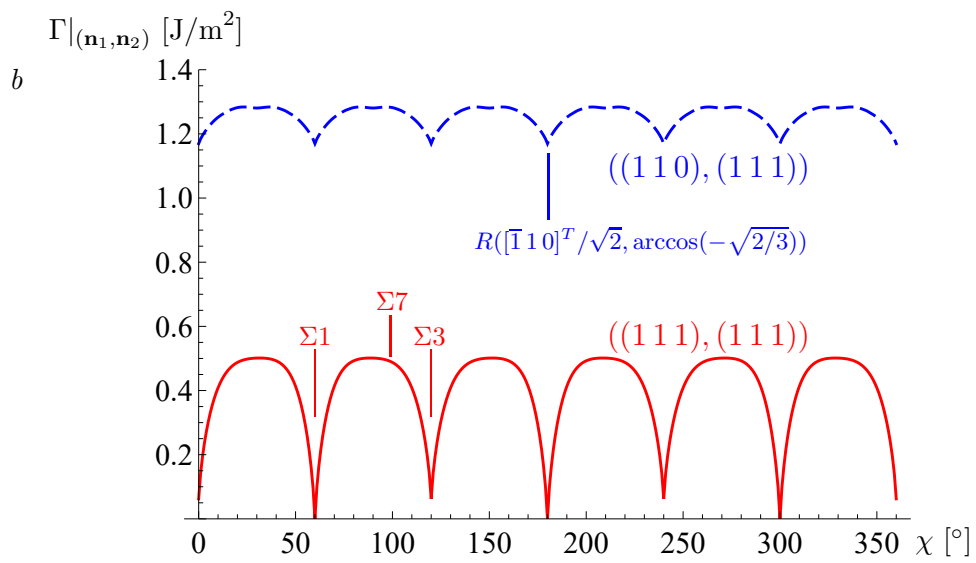
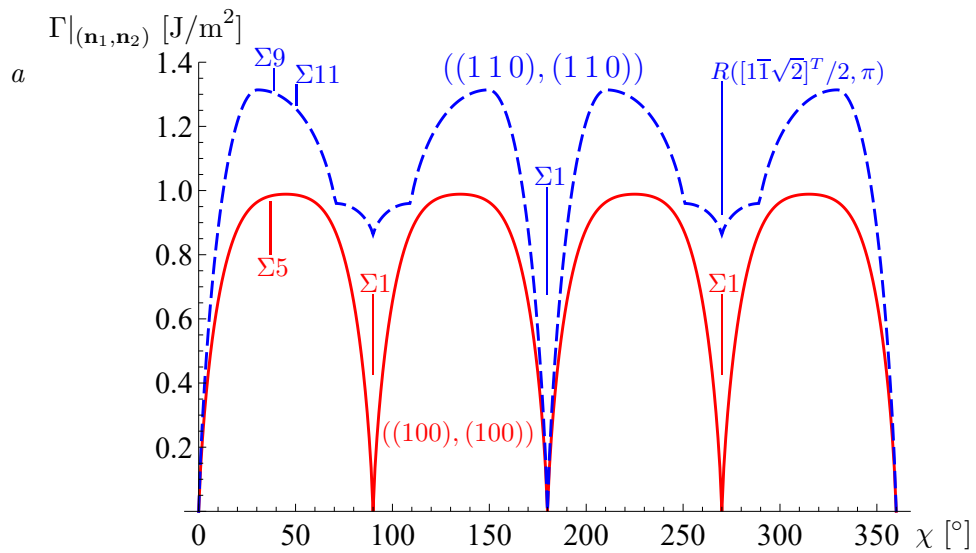
As an example, the dependence of the boundary free energy on the interface-plane parameters is considered. The celebrated Bulatov-Reed-Kumar (BRK) model [35] is used. It approximates atomic-scale simulation data taken from [36]. The case of Ni is inspected. The model is denoted here by Γ , and $\Gamma|_{(\mathbf{n}_1, \mathbf{n}_2)}$ denotes the restriction of Γ for fixed \mathbf{n}_1 and \mathbf{n}_2 and variable χ . Clearly, the function Γ takes the same values for equivalent boundary representations, and this holds not only for the equivalences (7) and (8) but also for (9).

With Γ expressed using the interface-plane parameterization, one can easily get the restriction $\Gamma|_{(\mathbf{n}_1, \mathbf{n}_2)}$ and look at the energies of boundaries with the planes characterized by \mathbf{n}_1 and \mathbf{n}_2 . Tab. 1 contains minimal, maximal and average values of $\Gamma|_{(\mathbf{n}_1, \mathbf{n}_2)}$ for a number of pairs $(\mathbf{n}_1, \mathbf{n}_2)$. It is noteworthy that the energy of boundaries formed by two (111) planes not only has a low average value, but also the maximum energy reached in this case is low. On the other hand, maximum energies of boundaries formed by two (110) planes or two (211) planes are high. The boundaries formed by (110) and (111) have high minimum and average energies. The last two rows of Tab. 1 for high-index boundary planes are to illustrate the lack of equivalence between the pairs $(\mathbf{n}_1, \mathbf{n}_2)$ and $(\mathbf{n}_1, -\mathbf{n}_2)$.

More detailed information is contained in plots of $\Gamma|_{(\mathbf{n}_1, \mathbf{n}_2)}$ versus χ . In the case of twist boundaries, such plots are closely related to frequently drawn plots of energy versus misorientation angle. In contrast, considerations regarding the dependence of the energy on the angle of rotation about axis perpendicular to the boundary plane for non-twist boundaries are difficult to find. Example plots of $\Gamma|_{(\mathbf{n}_1, \mathbf{n}_2)}$ versus χ are shown in Fig. 3. To make their symmetries clear, all figures are drawn in the domain from 0 to 2π . The functions in Fig. 3*a,b,c* have cusps, i.e., local minima at which $\Gamma|_{(\mathbf{n}_1, \mathbf{n}_2)}$ is not differentiable. In this regard, one needs to note that singularities in continuous energy models should arise from physical premises. Similarly to the case of surface energy and Wulff construction, there is a physical reason (related to boundary faceting) for cusps in energy as a function of vectors normal to the boundary plane [37]. However, the angle χ is independent of both \mathbf{n}_1 and \mathbf{n}_2 , and if one goes beyond $\Sigma 1$ and the twin boundary, there are no simple theoretical arguments for cusps in the dependence of $\Gamma|_{(\mathbf{n}_1, \mathbf{n}_2)}$ on χ and most of these functions could be free of singularities.

\mathbf{n}_1	\mathbf{n}_2	min	$\bar{\Gamma} _{(\mathbf{n}_1, \mathbf{n}_2)}$	max
(100)	(100)		0.80	0.99
(100)	(110)	0.90	1.24	1.37
(100)	(111)	0.76	0.96	1.02
(100)	(210)	1.23	1.27	1.30
(100)	(211)	1.00	1.14	1.17
(100)	(221)	0.78	1.10	1.27
(110)	(110)		1.07	1.31
(110)	(111)	1.17	1.26	1.28
(110)	(210)	1.03	1.11	1.17
(110)	(211)	0.87	1.20	1.29
(110)	(221)	1.04	1.19	1.30
(111)	(111)		0.41	0.50
(111)	(210)	1.17	1.24	1.31
(111)	(211)	0.90	1.14	1.27
(111)	(221)	0.89	1.08	1.23
(210)	(210)		1.11	1.35
(210)	(211)	1.05	1.19	1.30
(210)	(221)	0.94	1.21	1.33
(211)	(211)		1.12	1.35
(211)	(221)	0.59	1.13	1.29
(221)	(221)		1.09	1.30
(123)	(357)	0.65	1.13	1.30
(123)	($\bar{3}\bar{5}\bar{7}$)	0.33	1.16	1.30

Table 1: Energy of boundaries in Ni based on the BRK model for fixed \mathbf{n}_1 and \mathbf{n}_2 . $\bar{\Gamma}|_{(\mathbf{n}_1, \mathbf{n}_2)}$ is the energy averaged over χ , and min and max are the maximum and minimum values of $\Gamma|_{(\mathbf{n}_1, \mathbf{n}_2)}$, respectively. The min values in empty cells are zero; they correspond to the ‘no boundary’ case. The units are J/m². For brevity, the vectors \mathbf{n}_i are replaced by Miller indices of the boundary planes.



Continued on next page

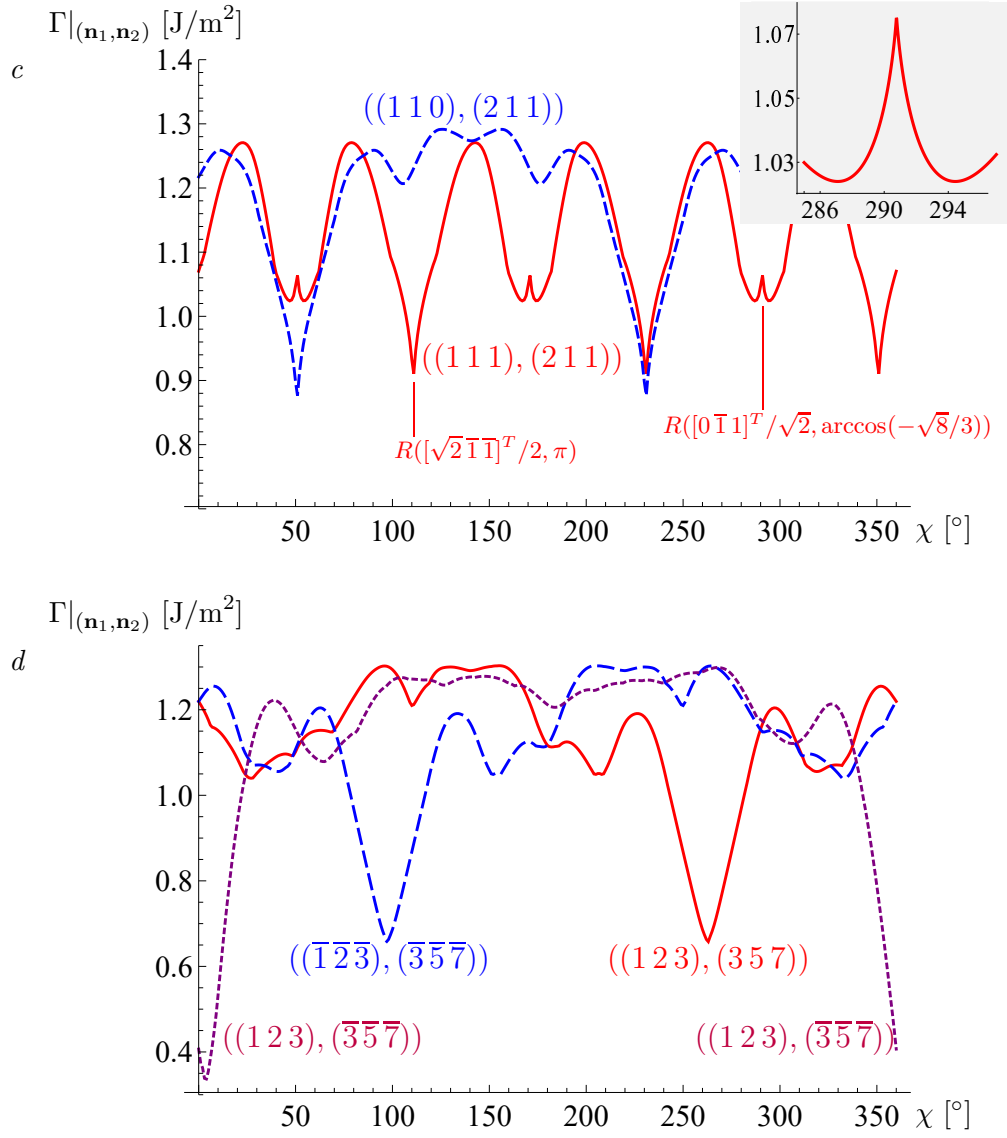


Figure 3: The grain boundary energy of Ni approximated by BRK model versus χ for selected \mathbf{n}_1 and \mathbf{n}_2 . Misorientations for some characteristic points are marked. The plots in (a) have the property that the point at $\chi = 0$ corresponds to the misorientation $\Sigma 1$. The inset in (c) shows the inverted cusp in magnification. Graphs in (d) illustrate the relationship (7) and lack of equivalence between $(\mathbf{n}_1, \mathbf{n}_2)$ and $(\mathbf{n}_1, -\mathbf{n}_2)$.

Interestingly, the plot for $(\mathbf{n}_1, \mathbf{n}_2) \sim ((111), (211))$ in Fig. 3c has an inverted cusp, i.e., a singular point which is a local maximum. Of the pairs $(\mathbf{n}_1, \mathbf{n}_2)$ listed in Tab. 1, inverted cusps are also in the plots for $((100), (210))$, $((110), (210))$, $((110), (221))$ and $((111), (221))$. This raises intriguing questions. Do the inverted cusps reflect properties of the input data or are due to other causes? Do other energy models constructed based on the same principles as BRK (e.g., [38–41]) have inverted cusps? How would inverted cusps affect physical properties of boundaries? What is the impact of inverted cusps on BRK-based grain growth simulations; see, e.g., [42–44]? Resolving these issues is beyond the scope of this study, but it is worth noting that the model described in [45] (which, by definition, has no singularities in the dependence on χ) shows local minima at positions of the BRK’s inverted cusps in four out of the five inspected cases, the only exception being $(\mathbf{n}_1, \mathbf{n}_2) \sim ((110), (210))$; see, Fig. 4. This seems to indicate that the presence of inverted cusps is an unintended feature of the BRK model.

For completeness, it is worth mentioning another natural way to visualize Γ by showing its dependence on one of the vectors \mathbf{n}_i when the other vector and χ are fixed. Such sections through Γ for selected \mathbf{n}_1 and χ and variable \mathbf{n}_2 are shown in Fig. 5. They resemble graphs plotted for a constant misorientation and variable \mathbf{n}_1 (see, e.g., [33]), but their interpretation is more complicated. The four-fold symmetry about \mathbf{e}_z visible in Fig. 5 is the direct result of (8). The function shown in Fig. 5b is also symmetric with respect the change of sign of \mathbf{n}_2 .

It has been suggested that properties of boundaries in cubic metals are controlled more by the boundary planes rather than misorientation; see, e.g., [16,47,48]. This claim is partly obscured by the fact that a change of one crystal plane with the other fixed is possible only by a change of misorientation. Since the angle χ is independent of both \mathbf{n}_1 and \mathbf{n}_2 , the interface-plane parameterization provides an opportunity to overcome this obscurity. The dimension of the subspace determined by \mathbf{n}_1 and \mathbf{n}_2 , which is four, is large compared to the dimension of the subspace defined by χ , which is one. This observation alone may lead to the conclusion that the influence of boundary planes is greater than the influence of misorientation. On the other hand, the level of control of a property by misorientation can be compared to that by boundary planes by looking at two distinct cases: one, with fixed \mathbf{n}_i ($i = 1, 2$) and variable χ , and second, with fixed misorientation M and variable angle, say ζ , representing a change of \mathbf{n}_1 . One may assume that the impact of a given parameter on a function is reflected in amplitude and frequency of changes in the function: the higher the impact, the larger and more frequent the changes. If the influence of the boundary plane on the boundary energy were larger than the influence of misorientation, the variation of

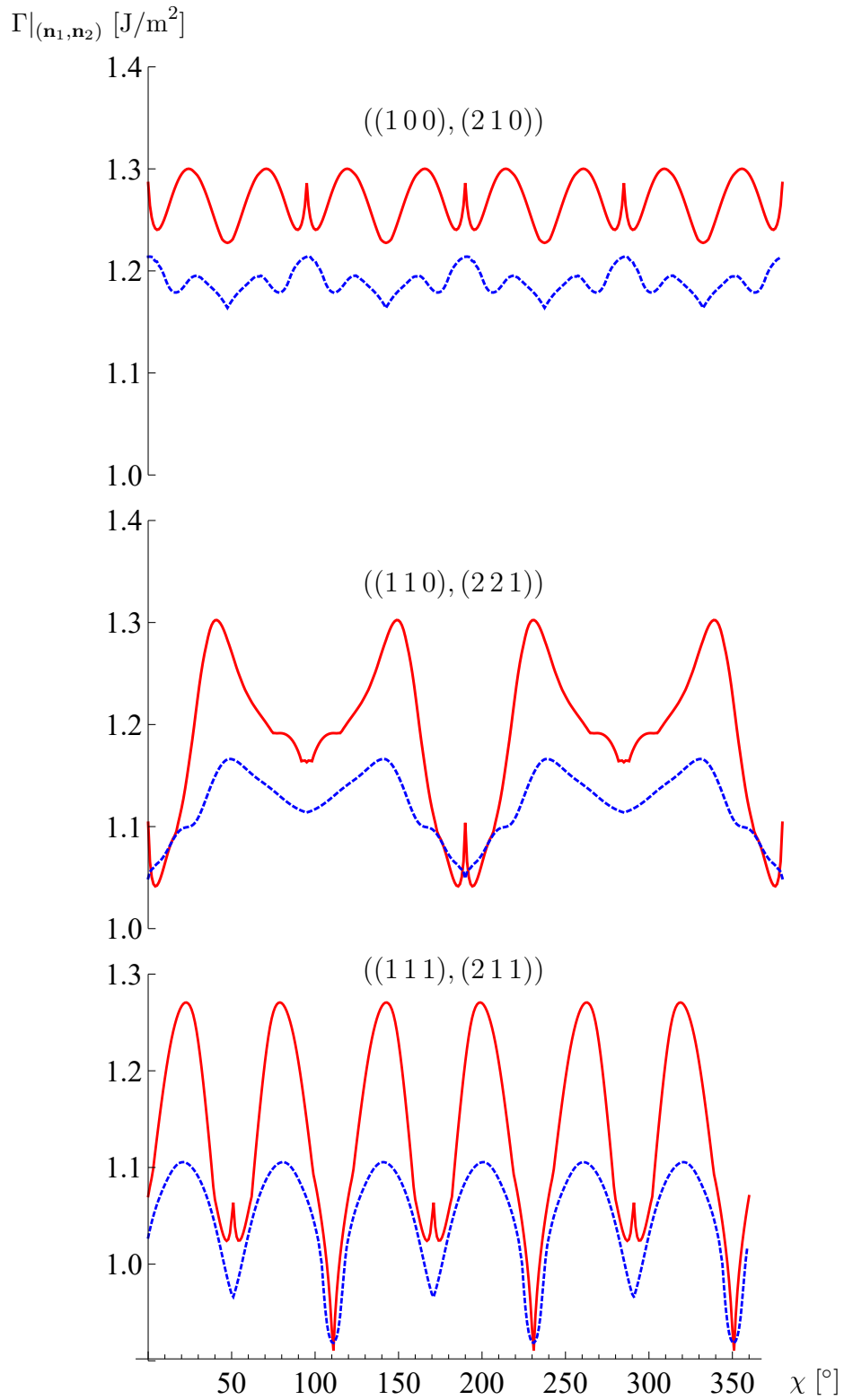


Figure 4: Selected BRK-based plots of $\Gamma|_{(n_1, n_2)}$ with inverted cusps (red, continuous) compared with corresponding data based on the model described in [45] (blue, dotted).

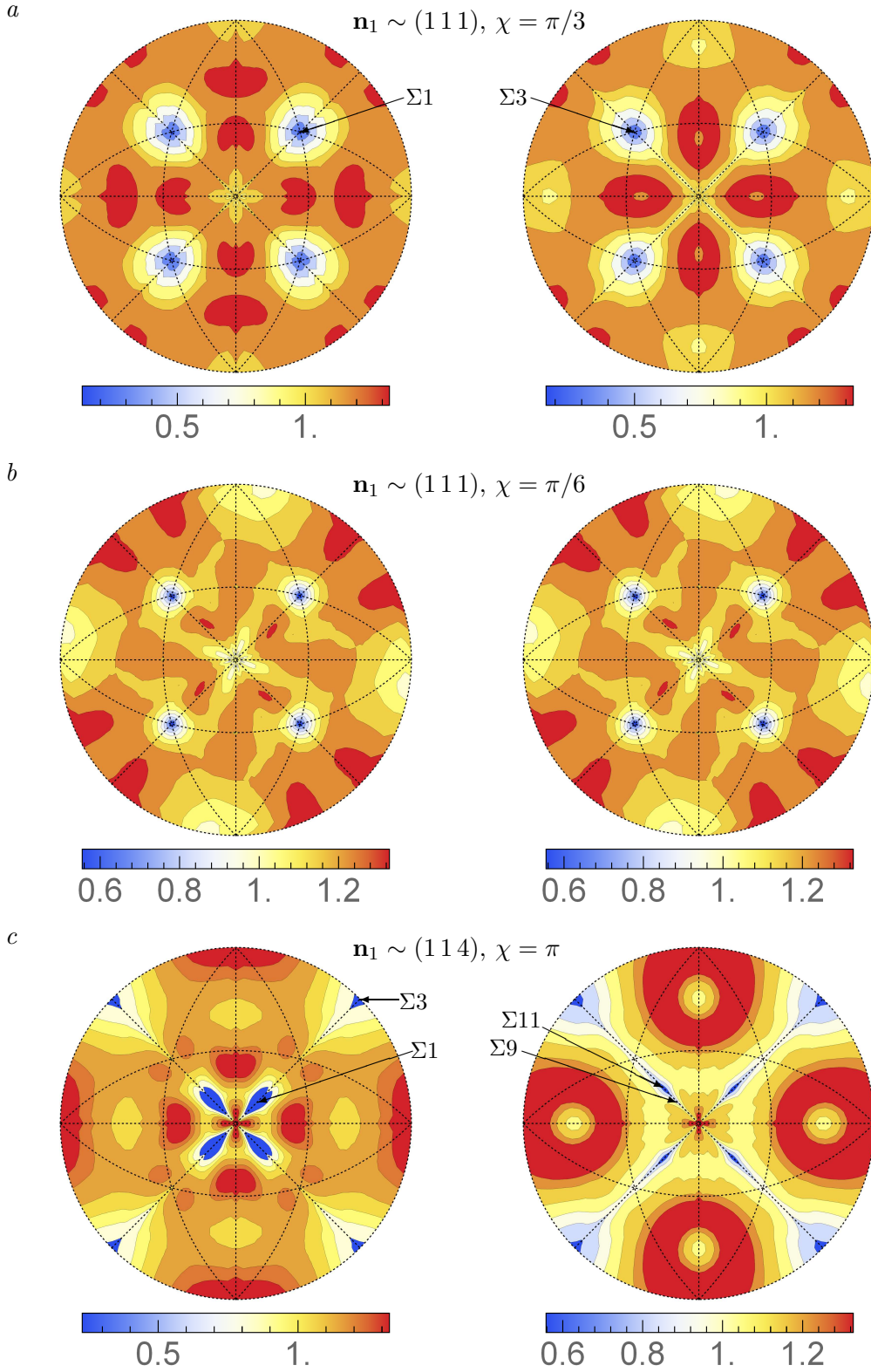


Figure 5: The grain boundary energy approximation of [35] for Ni versus \mathbf{n}_2 for selected \mathbf{n}_1 and χ . The plane corresponding to \mathbf{n}_1 and the angle χ are (111) and $\pi/3$ in (a), (111) and $\pi/6$ in (b) and (114) and π in (c). Left and right columns contain stereographic projections of the upper and lower hemispheres from the poles $-\mathbf{e}_z$ and $+\mathbf{e}_z$, respectively. Minima of the energy function at some low- Σ misorientations are marked. The energy unit is J/m^2 . The figures were drawn using code of Głowiński [46].

the energy function over ζ would be larger than the variation of the function over χ . A comparison of standard deviations from the means for twenty random energy plots with respect to each of χ and ζ shows the opposite. The standard deviations for the energy functions over χ were found to be on average more than twice as large as the deviations for the distributions over ζ . In other words, the comparison of variations of the energy over χ and ζ does not confirm the suggestion mentioned at the beginning of this paragraph.

5 Concluding remarks

Macroscopic parameters are an important tool in research on grain boundaries and inter-crystalline interfaces in general. Such parameters are not universal. Parameters useful in some circumstances may be inconvenient in other cases. Those facilitating interpersonal communication need to be easy to interpret and appeal to physical intuition. Using several different boundary parameterizations allows for looking at boundaries and functions defined on the boundary space from multiple perspectives.

The ‘interface-plane parameterization’ introduced in this paper is based on two vectors \mathbf{n}_i ($i = 1, 2$) identifying the orientation of the boundary plane in crystals on both sides of the boundary and the angle χ of rotation about the axis perpendicular to the plane, i.e., a boundary is represented by the triplet $(\mathbf{n}_1, \chi, \mathbf{n}_2)$. The triplet is directly linked to Euler angles representing crystal orientations. In many practical cases, the vectors \mathbf{n}_i ($i = 1, 2$) can be replaced by Miller indices.

The characterization of a boundary by the crystallographic planes is natural and intuitive. Also the rotation by the angle χ can be easily visualized, but capturing the configuration with $\chi = 0$ is generally complicated. Apart from simple special cases, it requires numerical calculations.

The interface-plane parameters of some characteristic boundary types are easy to interpret. This concerns symmetric boundaries represented by $(\mathbf{n}, \pi, -\mathbf{n})$, twist boundaries represented by $(\mathbf{n}, \chi, -\mathbf{n})$, and 180°-tilt boundaries represented by $(\mathbf{n}, \chi, \mathbf{n})$. However, the representation of general tilt boundaries is more involved.

An examination of the prominent Bulatov-Reed-Kumar [35] grain boundary energy model as a function of the interface-plane parameters revealed its previously unknown features. The energy dependence on χ shows inverted cusps for some pairs $(\mathbf{n}_1, \mathbf{n}_2)$. Standard deviations from the means for energy versus χ were found to be larger than for energy versus boundary plane changes, which is contrary to the assertion that boundary properties are controlled more by boundary planes than by misorientations.

For simplicity, the paper concerns homophase boundaries between centrosymmetric crys-

tals. However, from the viewpoint of macroscopic description, the cases of homo- and hetero-phase interfaces between centrosymmetric crystals differ in non-essential aspects. (There is no heterophase analogue to the ‘no-boundary’ case, and the exchange symmetry is forbidden.) Therefore, the scope of the described parameterization can be easily extended to interfaces between centrosymmetric crystals of different types.

There are no fundamental obstacles to abandoning the assumption of centrosymmetry and generalizing the interface-plane parameterization to interfaces between crystals with arbitrary point groups. With such a general approach, it would be necessary to separately consider the cases of centrosymmetric crystals, acentric but non-enantiomorphic crystals, and enantiomorphic crystals, as well as their combinations if inter-phase interfaces are taken into account.

Appendix A: Interface-plane parameters from interface matrix

The triplet $(\mathbf{n}_1, \chi, \mathbf{n}_2)$ or the parameters $\theta_1, \psi_1, \chi, \theta_2, \psi_2$ can be calculated from the interface matrix $\tilde{\mathbf{B}} = \mathbf{B}(M, \mathbf{n}_1)$ using elementary steps. The vectors \mathbf{n}_1 and \mathbf{n}_2 are directly accessible as parts of this matrix. The angles θ_i and ψ_i are obtained from \mathbf{n}_i ($i = 1, 2$) using

$$(\theta_1, \pi/2 - \psi_1) = \Theta^{-1}(+\mathbf{n}_1) \text{ and } (\theta_2, \pi/2 - \psi_2) = \Theta^{-1}(-\mathbf{n}_2), \quad (15)$$

where Θ^{-1} denotes the function inverse to Θ given in (6). Explicit expressions for spherical coordinates $(\theta, \varphi) = \Theta^{-1}(\mathbf{n})$ of the unit vector $\mathbf{n} = [n^1 n^2 n^3]^T$ are $\theta = \arccos(n^3)$ and $\varphi = \arctan(n^1, n^2)$ if $|n^3| \neq 1$ and $\varphi = 0$ otherwise.⁴

As for the determination of the angle χ , based on eq.(4), one has the relationship $\mathbf{Q}(\theta_1, \psi_1)^T \tilde{\mathbf{B}} \mathbf{Q}(\theta_2, \psi_2) = \mathbf{B}(R(\mathbf{e}_z, \chi), \mathbf{e}_z)$ or $Q(\theta_1, \psi_1)^T M Q(\theta_2, \psi_2) = R(\mathbf{e}_z, \chi) = P$, and hence, knowing θ_i, ψ_i and M , the angle is obtained via $\chi = \arctan(P_{11}, P_{12})$. Alternatively, the angle χ can be computed directly from the entries of $\tilde{\mathbf{B}} = \mathbf{B}(M, \mathbf{n}_1)$ without referring to θ_i and ψ_i by using

$$\begin{aligned} \chi &= \arctan(n_1^3 n_2^3 + M_{33}, M_{23} n_1^1 - M_{13} n_1^2) \text{ or} \\ \chi &= \arctan(n_1^3 n_2^3 + M_{33}, M_{32} n_2^1 - M_{31} n_2^2), \end{aligned}$$

where n_i^k is the k -th component of \mathbf{n}_i . The above relationships are applicable if $|n_i^3| \neq 1$.

⁴Two-argument arctan used here follows the convention that for $c > 0$ one has $\arctan(c \cos \alpha, c \sin \alpha) = \alpha$.

In the remaining cases, one has

$$\chi = \begin{cases} \arctan(\mp M_{13}, +M_{23}) & \text{if } n_1^3 = \pm 1 \text{ and } |n_2^3| \neq 1 , \\ \arctan(\pm M_{31}, -M_{32}) & \text{if } n_2^3 = \pm 1 \text{ and } |n_1^3| \neq 1 , \\ \arctan(\pm M_{11}, -M_{12}) & \text{if } n_1^3 = -1 \text{ and } n_2^3 = \pm 1 , \\ \arctan(\mp M_{11}, +M_{12}) & \text{if } n_1^3 = +1 \text{ and } n_2^3 = \pm 1 , \end{cases}$$

where either the lower or the upper signs are used concurrently.

Appendix B: Condition for tilt boundaries

In the case of a tilt boundary, the misorientation axis \mathbf{k} is perpendicular to \mathbf{n}_1 , i.e., $\mathbf{k} \cdot \mathbf{n}_1 = 0$. (This implies that also $\mathbf{k} \cdot \mathbf{n}_2 = 0$.) In terms of the parameters $(\theta_1, \psi_1, \chi, \theta_2, \psi_2)$, this condition has the form

$$q_c \cos \chi + q_s \sin \chi = 0 , \quad (16)$$

where

$$\begin{aligned} q_c &= \sin(\psi_1 - \psi_2) (\cos \theta_1 + \cos \theta_2) , \\ q_s &= \cos(\psi_1 - \psi_2) (\cos \theta_1 \cos \theta_2 + 1) + \sin \theta_1 \sin \theta_2 . \end{aligned}$$

Using the relationships (15) between (θ_i, ψ_i) and \mathbf{n}_i , one can express q_c and q_s through components of \mathbf{n}_i . If eq.(16) is satisfied, the misorientation axis is in the boundary plane or the misorientation angle is zero.

References

- [1] C. Goux. Etude de la structure et des propriétés des joints de grains à l'aide de bicristaux orientés en aluminium pur. *Mem. Sci. Rev. Metall.*, 58:661–675, 1961.
- [2] F.F. Lange. Mathematical characterization of a general bicrystal. *Acta Metall.*, 15:311–318, 1967.
- [3] M.A. Fortes. Grain boundary parameters. *Acta Cryst.*, A28:100–102, 1972.
- [4] C. Goux. Structure des joints de grains: considération cristallographiques et méthodes de calcul des structures. *Can. Metall. Quart.*, 13:9–31, 1974.
- [5] W. Zhu, G. Wu, A. Godfrey, S. Schmidt, Q. He, Z. Feng, T. Huang, L. Zhang, and X. Huang. Five-parameter grain boundary character distribution of gold nanoparticles based on three dimensional orientation mapping in the TEM. *Scripta Mater.*, 214:114677, 2022.
- [6] V.V. Korolev, J.J. Bean, Y.M. Nevolin, Y.V. Kucherinenko, K.P. McKenna, and P.V. Protsenko. Comparing five and lower-dimensional grain boundary character and energy distributions in copper: Experiment and molecular statics simulation. *Metall. Mater. Trans. A*, 53:449–459, 2022.
- [7] S. Patel, S. Goswami, P. Paul, F. Liu, S. Zheng, J.E. Sabisch, C. Duan, T. Venkatesan, H. Paik, H. Ding, P. Kazempoor, S. Xu, D. Ding, and I. Ghamarian. Orientation microscopy–assisted grain boundary analysis for protonic ceramic cell electrolytes. *J. Am. Ceram. Soc.*, 108:e20371, 2025.
- [8] Y. Zhang, E.D. Hansen, T. Harbison, S. Masengale, J. French, and L. Aagesen. A molecular dynamics survey of grain boundary energy in uranium dioxide and cerium dioxide. *J. Am. Ceram. Soc.*, 105:4471–4486, 2022.
- [9] E.R. Homer, G.L.W. Hart, C.B. Owens, D.M. Hensley, J.C. Spendlove, and L.H. Serafin. Examination of computed aluminum grain boundary structures and energies that span the 5D space of crystallographic character. *Acta Mater.*, 234:118006, 2022.
- [10] C. Wei, L. Zhang, J. Han, D.J. Srolovitz, and Y. Xiang. Grain boundary triple junction dynamics: A continuum disconnection model. *SIAM J. Appl. Math.*, 80:1101–1122, 2020.

- [11] B. Murgas, B. Flipon, N. Bozzolo, and M. Bernacki. Level-set modeling of grain growth in 316L stainless steel under different assumptions regarding grain boundary properties. *Materials*, 15, 2022.
- [12] G.B. Bizana and L.A. Barrales-Mora. Kinetics of grain boundary migration in nanosized Al polycrystals. *Acta Mater.*, 260:119261, 2023.
- [13] J.F. Panzarino, Z. Pan, and T.J. Rupert. Plasticity-induced restructuring of a nanocrystalline grain boundary network. *Acta Mater.*, 120:1–13, 2016.
- [14] P.H. Pumphrey. A plane matching theory of high angle grain boundary structure. *Scripta Metall.*, 6:107–114, 1972.
- [15] V. Randle. The role of the grain boundary plane in cubic polycrystals. *Acta Mater.*, 46:1459–1480, 1997.
- [16] V. Randle. ‘Special’ boundaries and grain boundary plane engineering. *Scripta Mater.*, 54:1011–1015, 2006.
- [17] W. Wang, S. Chen, G.S. Rohrer, and W. Chen. The inter-connections of $\Sigma 3$ boundaries in pure iron. *Scripta Mater.*, 128:18–22, 2017.
- [18] W. Wang, C. Cai, G.S. Rohrer, X. Gu, Y. Lin, S. Chen, and P. Dai. Grain boundary inter-connections in polycrystalline aluminum with random orientation. *Mater. Char.*, 144:411–423, 2018.
- [19] W. Wang, Y. Cui, G.S. Rohrer, C. Cai, S. Chen, X. Gu, and Y. Lin. Grain boundary inter-connections of $\Sigma 5$ boundaries in a high purity iron with a uniform microstructure. *Scripta Mater.*, 170:62–66, 2019.
- [20] D. Wolf and J.F. Lutsko. On the geometrical relationship between tilt and twist grain boundaries. *Z. Kristallogr.*, 189:239–262, 1989.
- [21] M. Takashima, A.D. Rollett, and P. Wynblatt. A representation method for grain-boundary character. *Philos. Mag. A*, 80:2457–2465, 2000.
- [22] A. Morawiec and K. Glowinski. On “macroscopic” characterization of mixed grain boundaries. *Acta Mater.*, 61:5756–5767, 2013.
- [23] A. Morawiec. On ‘interface-plane scheme’ and symmetric boundaries. *Z. Kristallogr.*, 227:199–206, 2012.

- [24] A. Morawiec. Symmetries of grain boundary distributions. In B. Adams, A. Rollett, and H. Weiland, editors, *Grain Growth in Polycrystalline Materials III*, pages 509–514, Warrendale, PA, US, 1998. TMS.
- [25] A. Morawiec. Models of uniformity for grain boundary distributions. *J. Appl. Cryst.*, 42:783–792, 2009.
- [26] A. Morawiec. *Orientations and Rotations. Computations in Crystallographic Textures*. Springer, Berlin, 2004.
- [27] D.L. Olmsted. A new class of metrics for the macroscopic crystallographic space of grain boundaries. *Acta Mater.*, 57:2793–2799, 2009.
- [28] T. Francis, I. Chesser, S. Singh, E.A. Holm, and M. De Graef. A geodesic octonion metric for grain boundaries. *Acta Mater.*, 166:135–147, 2019.
- [29] A.P. Sutton and R.W. Balluffi. *Interfaces in crystalline materials*. Oxford University Press, Oxford, UK, 1995.
- [30] H.J. Bunge. *Texture Analysis in Materials Science*. Butterworth’s, London, 1982.
- [31] A. Morawiec. Tilt and twist grain boundaries. *J. Appl. Cryst.*, 42:308–311, 2009.
- [32] D.M. Saylor, A. Morawiec, and G.S. Rohrer. Distribution and energies of grain boundaries in magnesia as a function of five degrees of freedom. *J. Amer. Ceram. Soc.*, 85:3081–3083, 2002.
- [33] D.M. Saylor, A. Morawiec, and G.S. Rohrer. The relative free energies of grain boundaries in magnesia as a function of five macroscopic parameters. *Acta Mater.*, 51:3675–3686, 2003.
- [34] Zhong X., D.J. Rowenhorst, H. Beladi, and G.S. Rohrer. The five-parameter grain boundary curvature distribution in an austenitic and ferritic steel. *Acta Mater.*, 123:136–145, 2017.
- [35] V.V. Bulatov, B.W. Reed, and M. Kumar. Grain boundary energy function for fcc metals. *Acta Mater.*, 65:161–175, 2014.
- [36] D.L. Olmsted, S.M. Foiles, and E.A. Holm. Survey of computed grain boundary properties in face-centered cubic metals: I. Grain boundary energy. *Acta Mater.*, 57:3694–3703, 2009.

- [37] C. Herring. Some theorems on the free energies of crystal surfaces. *Phys. Rev.*, 82:87, 1951.
- [38] H. Dette, J. Gösmann, C. Greiff, and R. Janisch. Efficient sampling in materials simulation-exploring the parameter space of grain boundaries. *Acta Mater.*, 125:145–155, 2017.
- [39] R. Sarochawikasit, C. Wang, P. Kumam, H. Beladi, T. Okita, G.S. Rohrer, and S. Ratanaphan. Grain boundary energy function for α iron. *Materialia*, 19:101186, 2021.
- [40] O. Chirayutthanasak, R. Sarochawikasit, A. Wisitsorasak, N. Rujisamphan, T. Frolov, T. Ooppelstrup, S. Dangtip, G.S. Rohrer, and S. Ratanaphan. Anisotropic grain boundary area and energy distributions in tungsten. *Scripta Mater.*, 209:114384, 2022.
- [41] O. Chirayutthanasak, R. Sarochawikasit, S. Khongpia, T. Okita, S. Dangtip, G.S. Rohrer, and S. Ratanaphan. Universal function for grain boundary energies in bcc metals. *Scripta Mater.*, 240:115821, 2024.
- [42] H. Hallberg and V.V. Bulatov. Modeling of grain growth under fully anisotropic grain boundary energy. *Model. Simul. Mater. Sc.*, 27:045002, 2019.
- [43] J.D. Niño and O.K. Johnson. Influence of grain boundary energy anisotropy on the evolution of grain boundary network structure during 3D anisotropic grain growth. *Comp. Mater. Sci.*, 217:111879, 2023.
- [44] J. Niño and O.K. Johnson. Evolution of crystallographic texture and grain boundary network structure during anisotropic grain growth. *Comp. Mater. Sci.*, 240:113023, 2024.
- [45] A. Morawiec. On modeling global grain boundary energy functions. *Acta Mater.*, 286:120697, 2025.
- [46] K. Głowiński. *Methods for quantitative characterization of three-dimensional grain boundary networks in polycrystalline materials*. PhD thesis, Polish Academy of Sciences, Institute of Metallurgy and Materials Science, 2015.
- [47] G.S. Rohrer. Grain boundary energy anisotropy: a review. *J. Mater. Sci.*, 46:5881–5895, 2011.
- [48] S. Ratanaphan, D.L. Olmsted, V.V. Bulatov, E.A. Holm, A.D. Rollett, and G.S. Rohrer. Grain boundary energies in body-centered cubic metals. *Acta Mater.*, 88:346–354, 2015.